

Physical Parameters of 11,100 Short-Period ASAS-SN Eclipsing Contact Binaries

XU-ZHI LI(李旭志) ^{1,2}, QING-FENG ZHU(朱青峰) ^{1,2,3}, XU DING(丁旭) ^{4,5,6}, XIAO-HUI XU(徐小慧)^{1,2},
HANG ZHENG(郑航)^{1,2}, JIN-SHENG QIU(邱锦盛)^{1,2} AND MING-CHAO LIU(刘明超) ^{4,7}

¹CAS Key Laboratory for Research in Galaxies and Cosmology, Department of Astronomy, University of Science and Technology of China, Hefei, 230026, China

²School of Astronomy and Space Sciences, University of Science and Technology of China, Hefei, 230026, China

³Deep Space Exploration Laboratory, Hefei 230088, China

⁴Yunnan Observatories, Chinese Academy of Sciences, 396 Yangfangwang, Guandu District, Kunming, 650216, Yunnan, P. R. China

⁵Key Laboratory of the Structure and Evolution of Celestial Objects, Chinese Academy of Sciences, P. O. Box 110, 650216 Kunming, P. R. China

⁶Center for Astronomical Mega-Science, Chinese Academy of Sciences, 20A Datun Road, Chaoyang District, Beijing 100012, P. R. China

⁷University of the Chinese Academy of Sciences, Yuquan Road 19, Shijingshan Block, Beijing, 100049, P. R. China

ABSTRACT

Starting from more than 11,200 short-period (less than 0.5 days) EW-type eclipsing binary candidates with the All-Sky Automated Survey for Supernovae (ASAS-SN) V-band light curves, we use MCMC and neural networks (NNs) to obtain the mass ratio (q), orbital inclination ($incl$), fill-out factor (f) and temperature ratio (T_s/T_p). After cross-matching with the Gaia DR3 database, the final sample contains parameters of 2,399 A-type and 8,712 W-type contact binaries (CBs). We present the distributions of parameters of these 11,111 short-period CBs. The mass ratio (q) and fill-out factor (f) are found to obey log-normal distributions, and the remaining parameters obey normal distributions. There is a significant period-temperature correlation of these CBs. Additionally, the temperature ratio (T_s/T_p) tends to increase as the orbital period decreases for W-type CBs. There is no significant correlation between them for A-type CBs. The mass ratio and fill-out factor ($q-f$) diagram suggest there is no significant correlation between these two parameters. A clear correlation exists between the mass ratio and radius ratio. The radius ratio increases with the mass ratio. Moreover, the deep fill-out CBs tend to fall on the upper boundary of the $q-R_s/R_p$ distribution, while the shallow fill-out CBs fall on the lower boundary.

Keywords: Eclipsing binary stars(444) — Contact binary stars(297) — Fundamental properties of stars(555)

1. INTRODUCTION

Contact binary systems (CBs) are close binaries in which both components fill their Roche lobes and share a common envelope (Kuiper 1941; Kopal 1959; Lucy 1968a,b). Previous studies have revealed that CBs whose components have similar temperatures (Kuiper 1941) are caused by the exchange of energy and mass transfer through the common envelope (Webbink 2003; Yakut & Eggleton 2005).

Most of the eclipsing CBs are EW-type eclipsing binary systems according to the morphological classification of light curves (Molík 1998; Li et al. 2020). Therefore, to understand the formation and evolution of CBs, EW-type eclipsing binaries are generally studied. The well-known period-luminosity-color (PLC) relations (Eggen 1967; Rucinski 1994; Chen et al. 2016, 2018b; Mateo & Rucinski 2017; Jayasinghe et al. 2020a; Qian et al. 2017, 2020) of CBs are established by using different passband photometric data of EW-type eclipsing binaries. The PLC relations are different between early- and late-type CBs (Jayasinghe et al. 2020a), and the PLC relations of different types of CBs have been extensively

studied (Graczyk et al. 2011; Pawlak et al. 2016; Rucinski 1994; Chen et al. 2016, 2018a,b; Mateo & Rucinski 2017; Jayasinghe et al. 2020a; Qian et al. 2017, 2020). In previous studies, early-type and late-type CBs are usually separated on the basis of their period. Late-type CBs generally have a period of less than 0.5 days and are much more numerous than early-type CBs. Chen et al. (2018a) defined the late-type CBs to have orbital periods $\log(P/d) \leq 0.25$, but Jayasinghe et al. (2020a) think that a period separation of $\log(P/d) \leq 0.30$ is a better choice. In this paper, we focus on late-type CBs, which are usually short-period CBs. Currently, statistical studies of CBs (Qian et al. 2017; Zhang et al. 2019; Sun et al. 2020; Jayasinghe et al. 2020a; Ren et al. 2021; Latković et al. 2021; Debski 2022) are becoming increasingly important thanks to the development of time-domain survey projects, e.g., the Catalina Sky Survey (CSS; Drake et al. 2009, 2014), the Wide-field Infrared Survey Explorer (WISE; Wright et al. 2010; Chen et al. 2018b), the Northern Sky Variability Survey (NSVS; Woźniak et al. 2004; Gettel et al. 2006), the Asteroid Terrestrial-impact Last Alert System (ATLAS; Heinze et al. 2018; Ren et al. 2021), the Optical Gravitational Lensing Experiment (OGLE; Udalski et al. 1992, 1994; Soszyński et al. 2016), the Zwicky Transient Facility (ZTF; Bellm et al. 2019; Chen et al. 2020), the All-Sky Automated Survey for Supernovae (ASAS-SN; Pojmanski 1997; Paczyński et al. 2006; Jayasinghe et al. 2018, 2019a), and some Space-based surveys like *Hipparcos* (Esa 1997), *Kepler* (Prša et al. 2011; Conroy et al. 2014; Kirk et al. 2016), *TESS* (Prša et al. 2022) and *Gaia* (Mowlavi et al. 2017, 2023).

The ASAS-SN (Shappee et al. 2014; Jayasinghe et al. 2018, 2019a,b, 2020b, 2021; Christy et al. 2023) is an automatic time-domain photometric sky survey project that currently consists of 24 telescopes distributed around the globe. More details can be seen on the websites¹. The ASAS-SN photometric down to $V \sim 17$ mag collected ~ 2000 to over 7500 epochs of V-band observations per field. The ASAS-SN Variable Stars Database² has revealed $\sim 688,000$ variable stars, $\sim 78,000$ of which are classified EW-type eclipsing binaries.

In this paper, we use the ASAS-SN V-band photometric light curves of EW-type eclipsing binaries to study short-period CBs. In section 2, we describe the sample selection and light curve analysis methods. In section 3, we give the parameter distribution and some discussion of these CBs. Finally, the summary and conclusion are presented in section 4.

2. SAMPLE SELECTION AND ANALYSIS OF THE LIGHT CURVES

2.1. Sample Selection

We used the ASAS-SN Variable Stars Database for target selection (Shappee et al. 2014; Jayasinghe et al. 2018, 2019a,b, 2020b, 2021). There are a total of 78,503 EW-type eclipsing binaries in the ASAS-SN Variable Stars Database. We search the short-period (less than 0.5 days) CB candidates under the following conditions. Based on the mean magnitude distribution of ASAS-SN (Jayasinghe et al. 2018), we select targets with mean V-band magnitude less than 15 mag, this includes the vast majority of targets. We also select targets with amplitudes greater than 0.2 mag because many ellipsoidal variable stars have amplitudes less than 0.2 mag and they are often mistaken for low-amplitude EW-type eclipsing binaries (Dal & Sipahi 2013; Li & Liu 2021; Skarka et al. 2022). The Laffler-Kinman string length (LkSL) statistic (Laffler & Kinman 1965; Clarke 2002) is a measure of scatter in the light curve of periodic variables. We used LKSL Statistic ≤ 0.1 to select the light curves of EW-type eclipsing binaries with good data quality. The class probabilities are given by Jayasinghe et al. (2018, 2019a), which are derived from a random forest classifier. They recommended that a class probability of > 0.9 is the best classification. Under these conditions, we selected 11,282 candidate targets. We downloaded ASAS-SN V-band light curve data from the ASAS-SN Variable Stars Database for these 11,282 targets, of which 4 targets had no data, and 11,278 targets had valid data.

2.2. Neural Network and MCMC Algorithm Model

Due to the development of time-domain photometric survey projects around the world, a large number of CB light curves have been released. It would be clearly impractical to use the Wilson-Devinney (Wilson & Devinney 1971; Wilson 1990; Van Hamme & Wilson 2007; Wilson et al. 2010; Wilson 2012) or PHOEBE (Prša et al. 2016) programs to derive the parameters of all these CBs. Prša et al. (2008) and Ding et al. (2021) used machine-learning methods to derive the parameters of detached binaries and contact binaries, respectively. These methods can speed up parameter derivation but cannot obtain the corresponding parameter errors.

¹ <https://www.astronomy.ohio-state.edu/asasn/index.shtml>

² <https://asas-sn.osu.edu/variables>

In this work, we use the neural network (NN) and the Markov chain Monte Carlo (MCMC) algorithm following the work in [Ding et al. \(2021, 2022\)](#) to derive the parameters of contact binaries. The NN model is trained with a set of light curves generated by Phoebe and known input parameters. Then, combined with the MCMC algorithm, the posterior distributions of the parameters can be quickly obtained. We used Phoebe to generate two sets (with or without the third light) of synthetic light curves as samples. The third light is one value for each light curve, representing the effect of the third body on the system as an equivalent result. In this step, the filter band is set to V because this work uses the ASAS-SN V-band data. The number of training light curves without and with the influence of the third light are 346,741 and 344,104, respectively. We select 10% of them as the test set. The model without the influence of the third light achieves a precision of 0.00045 magnitude in generating the light curves, while the model with the influence of the third light achieves a precision of 0.0002 magnitude in generating the light curves. Both models achieve a precision in generating the light curves that is less than 0.001 magnitude. Then, two models are obtained by training on the two sets of sample data. These two trained completed models can generate light curves according to the parameters of the CBs.

2.3. Analysis of the Light Curves

We downloaded ASAS-SN V-band light curve data from the ASAS-SN Variable Stars Database. We also obtained the period and primary eclipse time T_0 . Then, we phased these data and turned them into phase-magnitude data. To determine the fundamental photometric parameters of these ASAS-SN short-period CBs, the light curves were analyzed by using the NNs and MCMC algorithms.

We apply the two obtained models (with or without the third light) to obtain the parameters of the phased ASAS-SN light curves. Before using the models, we calculate the temperature for these CBs based on the given period-temperature relationship by [Jayasinghe et al. \(2020a\)](#) as follow:

$$T_{eff} = 6598 + 5260 * \log_{10}(P/0.5)K. \quad (1)$$

We use the parameter of goodness-of-fit (R^2) to evaluate the relevant results. The goodness-of-fit (R^2) is calculated based on the light curves generated by Phoebe and the original phased ASAS-SN light curves. If one target fits better under the third light model and the luminosity ratio of the third light

$$L_3/(L_1 + L_2 + L_3) \geq 0.2, \quad (2)$$

we consider the third light present and use the third light fitting model. The non-third-light model was used for the rest of the cases.

We have listed four example targets, the observations and best-fitting solutions of the light curves are displayed in Figure 1. We select all targets with goodness-of-fit (R^2) greater than 0.8, with a total of 11,145 short-period ASAS-SN CBs. The sky distribution of the short-period CBs in ASAS-SN, colored by their period, is shown in Figure 2.

2.4. Final sample

Based on the analysis with the machine learning method (NN and MCMC algorithm model), we obtained the system parameters of ASAS-SN short-period CBs. The initial effective temperature of the first substar (T_1) is calculated by the period-temperature relationship ([Jayasinghe et al. 2020a](#)). The orbital inclination ($incl$), mass ratio (q), temperature ratio (T_2/T_1), fill-out factor (f), third light ratio (l_3) and corresponding errors are derived by the machine learning method. The relative radii of the two substars (r_1, r_2) and luminosity ratio (L_2/L_1) are determined by Phoebe.

We define mass ratio as values between 0 and 1, with the more massive star being the primary star and the less massive star being the secondary star. Thus, when the derived mass ratio (q) is greater than 1, we take the reciprocal as the final mass ratio. Similarly, the reciprocal of the temperature ratio T_2/T_1 and luminosity ratio L_2/L_1 should be T_s/T_p and L_s/L_p , respectively. The radius r_1, r_2 should be exchanged as R_s, R_p , and the rest of the parameters do not need to be changed.

We cross-matched the CBs with Gaia DR3 ([Gaia Collaboration et al. 2023](#)) using a matching radius of 5.0 arcsec to obtain the temperature of the primary stars (T_p). Finally, we matched a total of 11,111 targets, of which 9,621 could obtain the temperatures (T_{eff}) from Gaia DR3. For the remaining 1490 targets, we still use the calculated temperature by the period-temperature relationship ([Jayasinghe et al. 2020a](#)) as the primary star temperature. The final parameters for these CBs are given in the attached table in catalog format. The information listed in Table 1 is an introduction to the contents of catalog-1.

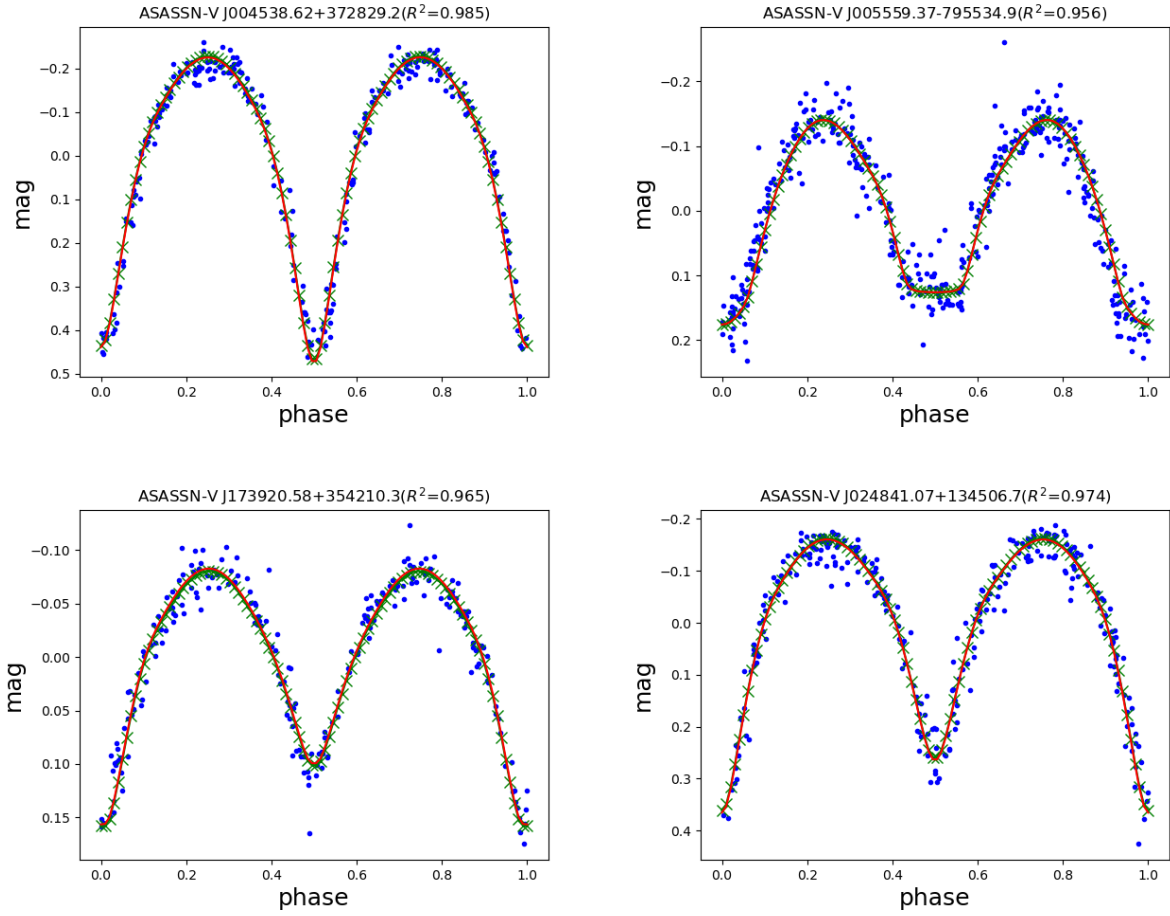


Figure 1. The blue dots represent the phased ASAS-SN light curves. Using the NNs and MCMC algorithm model to obtain the posterior distribution of the parameters as the input parameters. The red line represent the light curves generated by the NNs model with the input parameters. The green X line and symbol represent the light curves generated by Phoebe using the same input parameters. Top row: two example targets used the non-third-light model to get the parameters. Bottom row: two example targets used the third light model to get the parameters, and the luminosity ratio of the third light are about 68% and 27%, respectively.

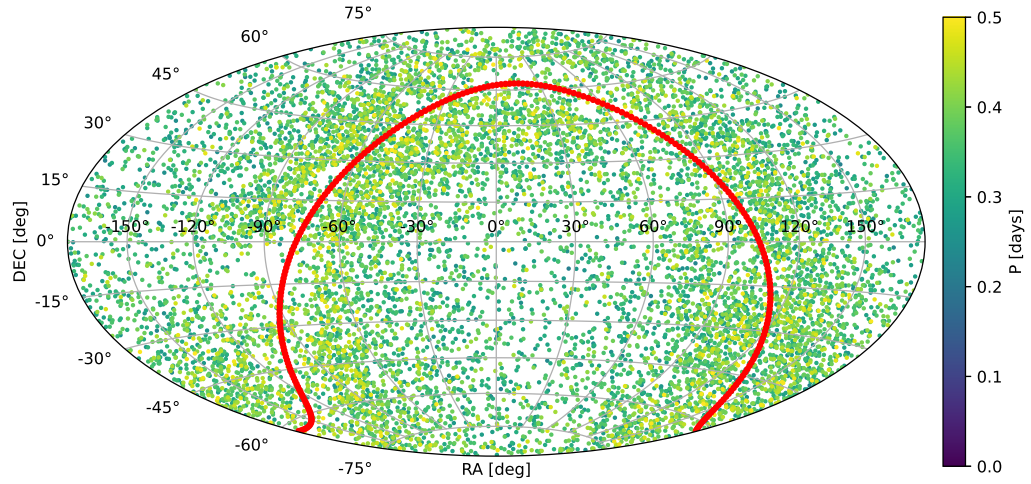


Figure 2. Projected distribution of the 11,145 short-period ASAS-SN contact binaries in equatorial coordinates (Hammer projection). The points are colored by period. The red line indicates the Galactic plane.

Table 1. Contents of the catalog-1 with 11,111 CBs

Num	Label	Units	Explanations
1	name		ASAS-SN Name
2	RA	◦	RA (J2000)
3	Dec	◦	DEC (J2000)
4	Period	day	Orbital period
5	T_p	K	Effective temperature of the primary star
6	$incl$	◦	Orbital inclination
7	σ_i	◦	Uncertainty in $incl$
8	q		Mass ratio, $q = \frac{m_s}{m_p} \leq 1$
9	σ_q		Uncertainty in q
10	f		Fill-out factor. $f = \frac{\Omega_{in} - \Omega}{\Omega_{in} - \Omega_{out}}$, where Ω_{in} and Ω_{out} are the inner and outer Lagrangian surface potential values, surface potential $\Omega = \Omega_1 = \Omega_2$.
11	σ_f		Uncertainty in f
12	T_s/T_p		Temperature ratio
13	T_s	K	Effective temperature of the secondary star
14	Type		CBs subtype classification (A or W)
15	R_p		Relative radius of the primary star
16	R_s		Relative radius of the secondary star
17	L_s/L_p		Luminosity ratio
18	l_3		Third light ratio $l_3 = L_3/(L_1 + L_2 + L_3)$
19	R^2		Goodness of fit
20	DR3Name		Gaia DR3 ID
21	T_{eff}	K	Effective temperature from Gaia DR3

3. PARAMETER DISTRIBUTION AND DISCUSSION

In the previous section, we obtained physical parameters of 11,111 ASAS-SN short-period CBs. The physical parameters include orbital period ($Period$), temperatures of the primary stars and the secondary stars (T_p , T_s), mass ratio (q), orbital inclination ($incl$), fill-out factor (f), temperature ratio (T_s/T_p), relative radii of the two substars (R_p , R_s), luminosity ratio (L_s/L_p). Here, we show the distribution of each parameter.

3.1. Parameter distribution

Figure 3 show the distribution of orbital periods (p), temperature (T_p , T_s), temperature ratio (T_s/T_p), orbital inclination ($incl$), fill-out factor (f), mass ratio (q) and relative radius (R_p , R_s) for the 11,111 ASAS-SN short-period CBs. The period distribution of ASAS-SN short-period CBs peaks at approximately 0.35 d, which is slightly shifted from the typical distribution of short-period EW-type eclipsing binaries with a peak at 0.31 d (Qian et al. 2020; Jayasinghe et al. 2020a). This may be caused by the fact that some short-period ellipsoidal variable stars are usually classified as EW-type eclipsing binaries. Ellipsoidal variable stars and low amplitude EW-type eclipsing binaries are not easily distinguished directly by light curves (Dal & Sipahi 2013; Li & Liu 2021; Skarka et al. 2022). However, in this paper, the selection of our sample with amplitudes greater than 0.2 mag, which has led to the early exclusion of many ellipsoidal variable stars that have been misclassified as low amplitude EW-type eclipsing binaries.

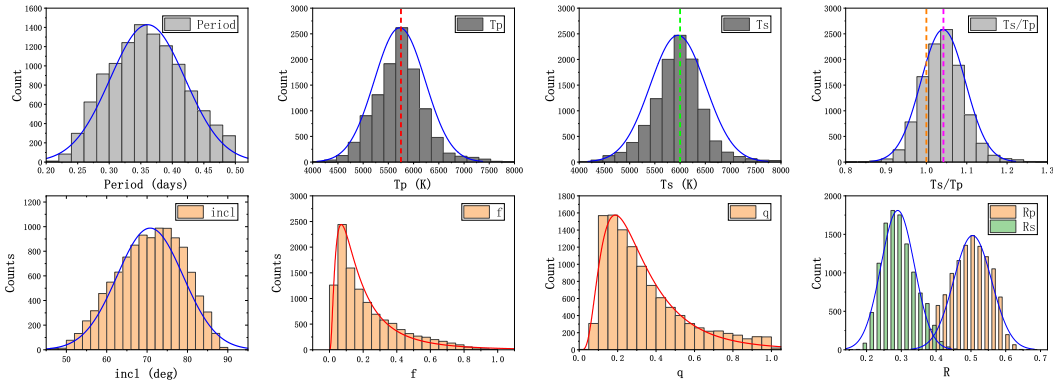


Figure 3. Distribution of orbital periods (period), temperature (T_p , T_s), temperature ratio (T_s/T_p), orbital inclination ($incl$), fill-out factor (f), mass ratio (q) and relative radius (R_p , R_s) for the 11,111 ASAS-SN short-period CBs. The period distribution have a peak around 0.35 d. The temperature distribution of primary and secondary stars peaks at approximately 5750 K (the red short dashed lines) and 6000 K (the green short dashed lines), respectively. The orange short dashed lines represents a temperature ratio of 1, the left side represents the A-type CBs and the right side represents the W-type CBs. The distributions of the orbital period, temperature (T_p , T_s), temperature ratio (T_s/T_p), inclination ($incl$) and relative radius (R_p , R_s) roughly obey normal distributions (the blue solid line), the distributions of the mass ratio (q) and the fill-out factor (f) obey log-normal distributions (the red solid line).

The temperature distribution of ASAS-SN short-period CBs peaks at approximately 5750 K (the red short dashed lines) for the primary star and 6000 K (the green short dashed lines) for the secondary star. The peak of the secondary star temperature is higher than the peak of the primary star temperature, as can also be seen from the temperature ratio distribution. Traditionally, CBs have been classified into two subtypes based on temperature: A-type and W-type (Binnendijk 1970). In A-type the more massive star is hotter, while in W-type the more massive star is cooler. Our sample contains 2,399 A-type and 8,712 W-type CBs.

The orbital inclination distribution indicates that most CBs have orbital inclinations larger than 50° , which is likely due to selection effects, and CBs with high orbital inclination are more easily observed. Another reason is that our method is more reliable when used to fit targets with orbital inclinations greater than 50° (Ding et al. 2021). The fill-out factor distribution of ASAS-SN short-period CBs indicates that CBs generally have shallow fill-out. The mass ratio distribution indicates that both extremely low mass ratio ($q \leq 0.1$) and large mass ratio ($q \geq 0.7$) CBs are less frequent.

Very interestingly, according to the distribution of these short-period CB parameters, we find that only the distributions of the mass ratio and the fill-out factor obey log-normal distributions, while the rest of the parameters

roughly obey normal distributions. We are confident that this is related to the evolution of contact binaries, but more simulation work is needed to confirm this.

3.2. *Period-Luminosity-Color Relations*

Figure 4 is a 2D kernel density graph. There is a clear correlation between the orbital period and the temperature of the primary star. The period-temperature relationship is actually the well-known period-color relationship or the so-called period-luminosity-color (PLC) relations (Eggen 1967; Rucinski 1994; Chen et al. 2016, 2018b; Mateo & Rucinski 2017; Jayasinghe et al. 2020a; Qian et al. 2017, 2020). Most CBs are located in a banded region rather than a simple linear PLC. This is related to the evolution of the common envelope of CBs, where the fill-out factor affects the PLC (Qian et al. 2020).

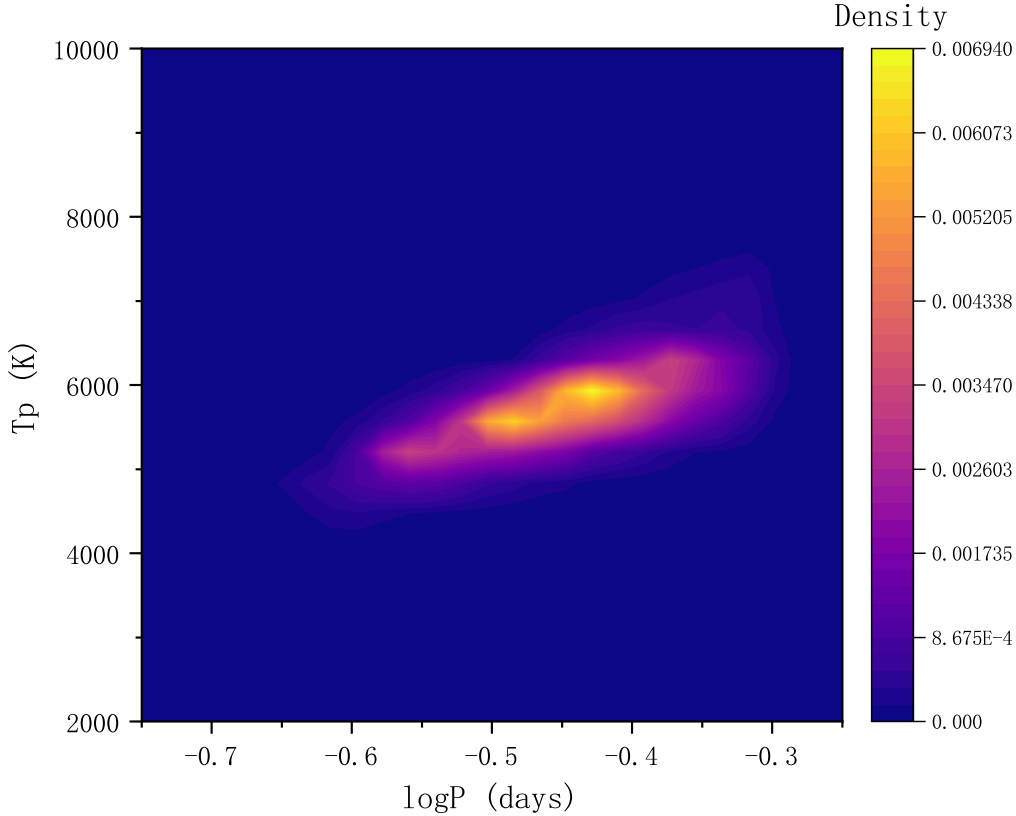


Figure 4. The 2D kernel density graph between the orbital period and the temperature of the primary stars. It shows a clear correlation between the orbital period and the temperature of short-period CBs (usually are the late-type CBs), the longer the period, the higher the temperature.

3.3. *Period and Subtype CBs Evolution*

We plot the 2D kernel density graph between the orbital period and the temperature ratio, as shown in Figure 5. The period-temperature ratio seems to have some trend of correlation, as shown by the black line with arrows in Figure 5. As shown in Figure 5, there are far more W-type samples than A-type samples in the short-period CBs. For A-type CBs, there is no significant relationship between the temperature ratio and period, similar to a random distribution; however, for W-type CBs, the temperature ratio tends to increase as the orbital period decreases. This suggests that the evolution of A-type CBs is different from that of W-type CBs. Perhaps this could indicate that A-type CBs may be less evolved and suggest that W-type CBs evolved from A-type CBs (Li et al. 2020; Zhang et al. 2020). Currently, the formation and evolution of CBs are still open issues (Yakut & Eggleton 2005; Gazeas & Stępień 2008; Li et al.

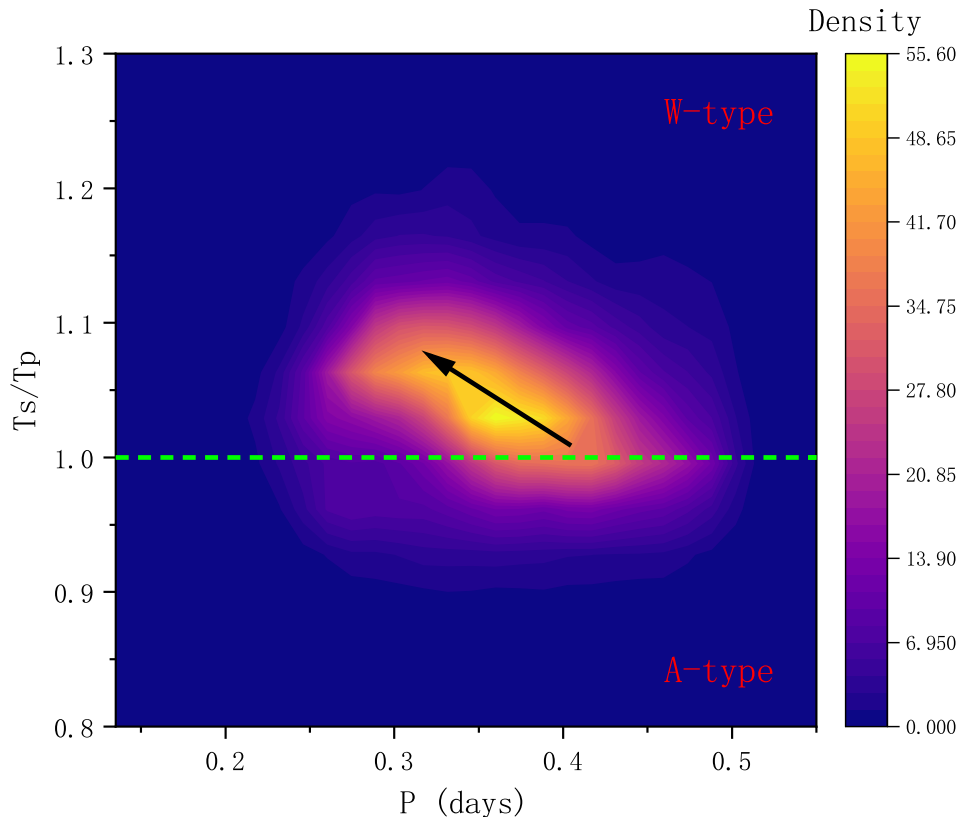


Figure 5. The 2D kernel density graph between the orbital period and the temperature ratio. The green short dashed lines represent the temperature ratio as 1. The upper and lower parts of the short dashed lines represent the W-type and the A-type CBs, respectively.

2007, 2008; Stępień 2009; Yıldız 2014; Qian et al. 2017, 2018; Jiang 2020; Maceroni & van't Veer 1996; Awadalla & Hanna 2005; Eker et al. 2006; Gazeas & Niarchos 2006; Yıldız & Doğan 2013).

Figure 6 shows the correlation between the orbital period and the temperature, mass ratio, orbital inclination and fill-out factor. This shows that they do not have a good correlation with the period, except for temperature. In addition, we find that the temperature, mass ratio, orbital inclination and fill-out factor are independently distributed from each other. There is no correlation among them.

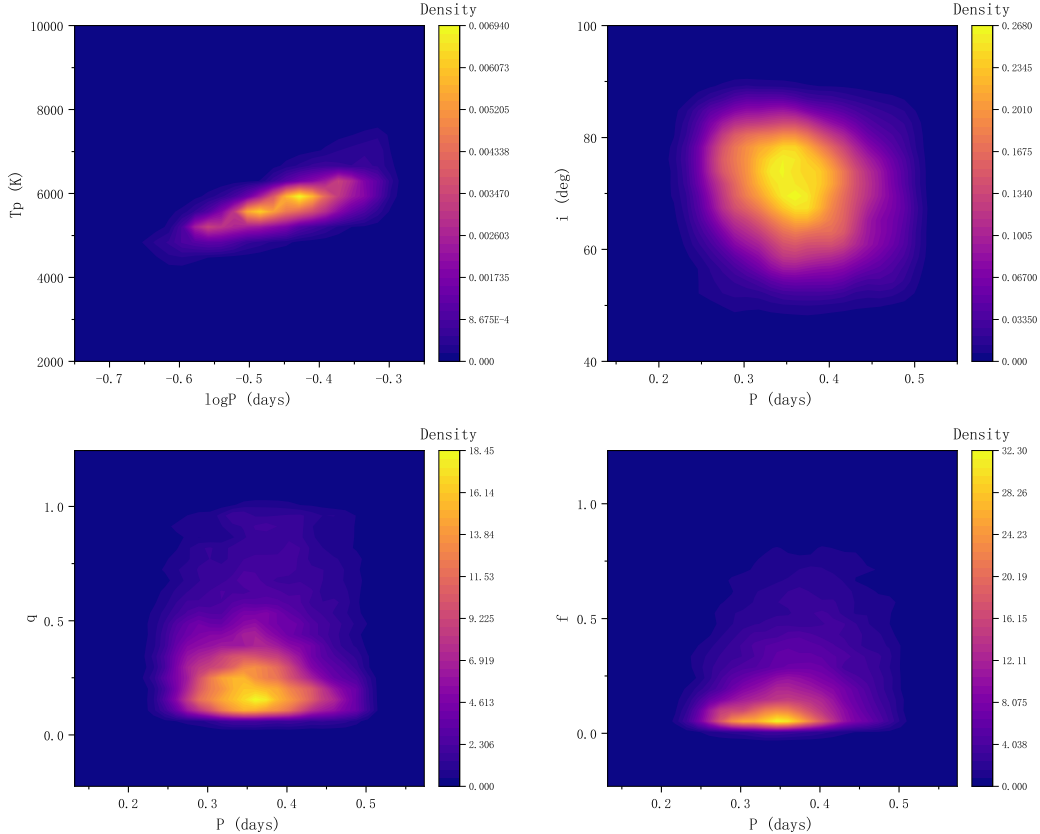


Figure 6. The 2D kernel density graph between the orbital period and the temperature, mass ratio, orbital inclination and fill-out factor. There are no certain correlations between orbital period with mass ratio, orbital inclination and fill-out factor.

3.4. q - f Diagram

Figure 7 shows the correlation between the mass ratio and fill-out factor of ASAS-SN short-period CBs. As shown in Figure 3 and discussed in section 3.1, we find that the distributions of the mass ratio and the fill-out factor obey log-normal distributions. The correlation between the mass ratio and the fill-out factor is weak, as shown in Figure 7. However, we can also find much useful information in the $q - f$ diagram.

In recent decades, there have been several studies on deep, low-mass ratio contact binaries (DLMRCBs) with mass ratios and fill-out factors of $q < 0.25$ and $f > 50\%$ (Yang & Qian 2015; Zhou et al. 2016; Li et al. 2021, 2022), corresponding to the upper left region in Figure 7. Model calculations suggest that these DLMRCBs will finally merge into single stars, such as blue stragglers or FK-Com-type stars (Stepien 2006; Stepień 2011). V1309 Sco, the only observed sample, was a DLMRCB before the merge and was recently found as a blue straggler (Tylenda et al. 2011; Zhu et al. 2016; Ferreira et al. 2019). Recently, Gazeas et al. (2021) and Loukaidou et al. (2022) led a project focusing on DLMRCBs. They find that low mass-ratio systems seem more likely to eventually merge into single fast-rotating stars. Our DLMRCB samples are located in the upper left region in Figure 7, and they should also be candidates for merging.

As shown in Figure 7, there is no clear correlation between the mass ratio and fill-out factor. However, it shows the upper limit of the fill-out factor increases as the mass ratio decreases, as shown by the green solid line in the figure, which is consistent with our previous results (Li et al. 2020). In the previous study we had a sample of only 380 *Kepler* CBs, this time we have a much larger sample.

We can also see in Figure 7 that there are very few samples in the upper right region that contain CBs with a deep fill-out factor and high mass ratio ($q > 0.25$ and $f > 50\%$). The common convective envelope-dominated mechanism

(Liu et al. 2018) can explain the presence of short period, deep fill-out factor and high mass ratio CBs. According to the CCE-dominated mechanism, P will becomes very short when f is large at a high value of q .

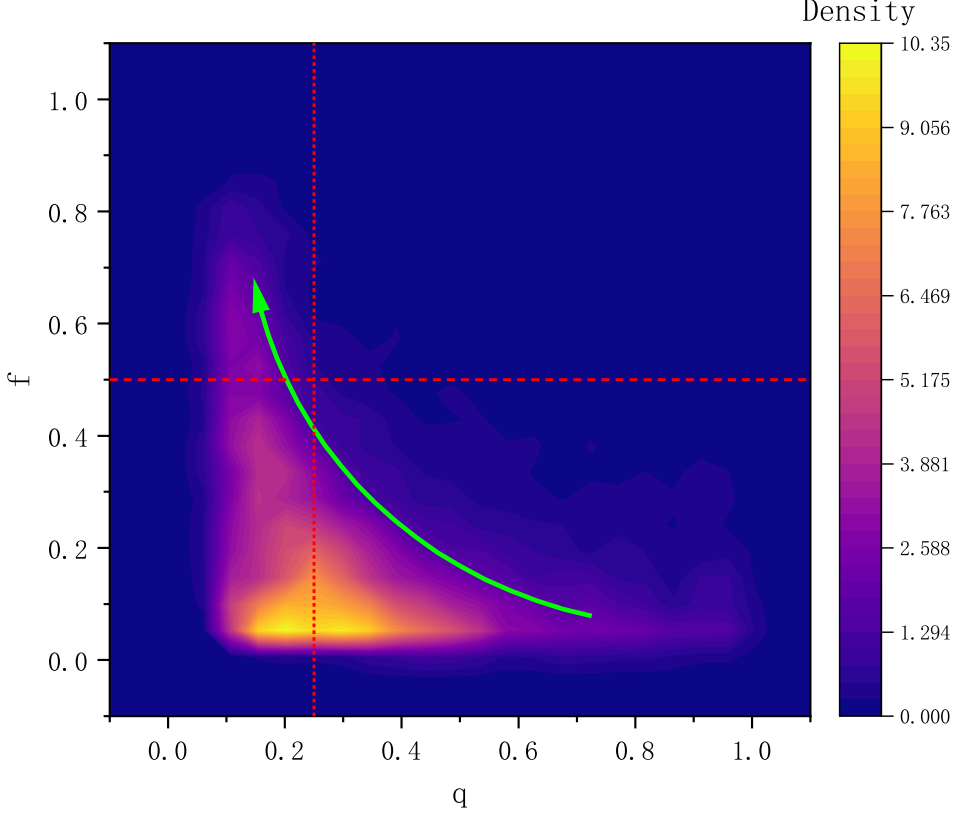


Figure 7. The 2D kernel density graph between the mass ratio and fill-out factor of ASAS-SN short-period CBs. The red horizontal short dashed lines and vertical short dashed lines represent fill-out factor of 0.5 and mass ratio of 0.25, respectively. The green solid line indicates the trend between mass ratio (q) and fill-out factor (f). There are very few sample in the upper right region, thus CBs with deep fill-out factor, high mass ratio are more worthy of attention and study.

3.5. Mass ratio - radius ratio Relationship

The mass-radius relation ($M - R$) and mass-luminosity relation ($M - L$) of the primary and secondary stars of CBs have been studied by many authors (Yakut & Eggleton 2005; Li et al. 2008; Yildiz & Doğan 2013; Li et al. 2020; Latković et al. 2021). The $M - R$ relation of a CB system is significantly different from that of a single zero main sequence star. An approximate relation between the radii and masses of the components is $\frac{R_s}{R_p} = q^{0.46}$ (Kuiper 1941), while for the zero main sequence star the relation is $\frac{R_s}{R_p} = q^{0.6}$ (Lucy 1968a).

We used the obtained data to fit the $q - R_s/R_p$ relation, and the results are shown as the red solid line in Figure 8 as $R_s/R_p = q^{0.435}$, which is very close to the results in Kuiper (1941). The relationship between R_s/R_p and q is monotonically increasing overall, but with dispersion at all q -value locations. We fit the upper and lower bounds of this region, as shown in the black and magenta solid lines in Figure 8. The black solid line has a relation of $R_s/R_p = q^{0.38}$, while the magenta solid line has $R_s/R_p = q^{0.48}$. We find that the upper bound region is the deep fill-out CBs and the lower bound region is the shallow fill-out CBs. This suggests that the radius ratio is related to the fill-out factor of CBs for the same mass ratio (Yakut & Eggleton 2005).

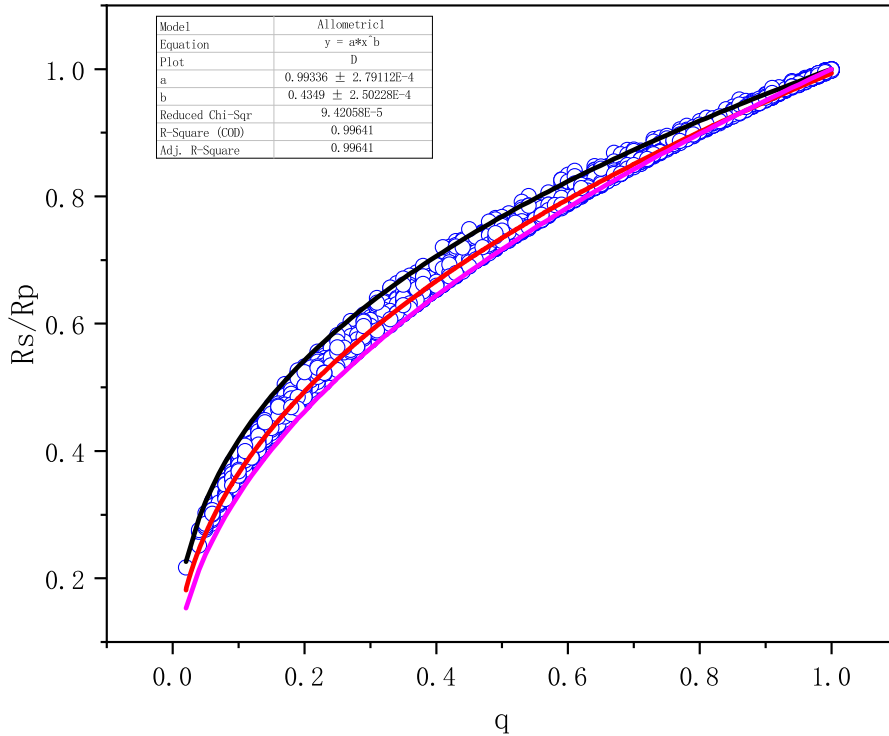


Figure 8. Mass-radius Relationship of our short-period CBs. The red solid line represents the best fitting result as $R_s/R_p=q^{0.435}$. The black solid line represents the fitting result as $R_s/R_p=q^{0.38}$ for the upper bound, and the magenta solid line represents the fitting result as $R_s/R_p=q^{0.48}$ for the lower bound. The upper bound region is the deep fill-out CBs and the lower bound region is the shallow fill-out CBs.

4. SUMMARY AND CONCLUSIONS

In this paper, we present the physical parameters of 11,111 short-period (see catalog-1) eclipsing contact binaries from the All-Sky Automated Survey for Supernovae (ASAS-SN) based on a machine learning method with neural networks (NNs) and Markov chain Monte Carlo (MCMC) algorithms. Based on the Gaia DR3 database, statistical work was performed for these ASAS-SN short-period CBs. Our main results and conclusions are summarized below.

1. After cross-matching with the Gaia DR3 database, our final sample contained 11,111 CBs, with a period less than 0.5 d, they were classified into two subtypes: 2,399 A-type and 8,712 W-type CBs.

2. We present the distributions of parameters of these short-period CBs, where the distributions of the mass ratio (q) and fill-out factor (f) are found to obey log-normal distributions, and the remaining parameters obey normal distributions.

3. There is a clear correlation between the orbital period and the temperature of short-period CBs, which is the well-known period-luminosity-color (PLC) relations.

4. Different subtypes of CBs seem to have different period and temperature ratio relationships. For A-type CBs, there is no significant correlation between the temperature ratio and period, similar to a random distribution; however, for W-type CBs, the temperature ratio tends to increase as the orbital period decreases. This likely suggests that the evolution of A-type CBs is different from that of W-type CBs.

5. The $q - f$ diagram indicated that there is no significant correlation between the mass ratio and fill-out factor. However, it can be seen that the fill-out factor increases as the mass ratio decreases.

6. The mass ratio - radius ratio ($q - R_s/R_p$) diagram indicated that there is a clear correlation between the mass ratio and radius ratio, the radius ratio increases with the mass ratio. And this correlation is also related to the fill-out

factor of CBs, the deep fill-out CBs fall on the upper boundary of the $q-R_s/R_p$ distribution, while the shallow fill-out CBs fall on the lower boundary.

This work is supported by the National Key Research and Development Program of China (2023YFA1608100), the Anhui Provincial Natural Science Foundation (2308085QA35), the Strategic Priority Research Program of the Chinese Academy of Sciences (No. XDB 41000000), the China Postdoctoral Science Foundation (2021M703099) and the Fundamental Research Funds for the Central Universities.

This work made use of data from the ASAS-SN Variable Stars Database (<https://asas-sn.osu.edu/variables>). ASAS-SN is funded in part by the Gordon and Betty Moore Foundation through grants GBMF5490 and GBMF10501 to the Ohio State University and funded in part by the Alfred P. Sloan Foundation grant G-2021-14192.

This work has made use of the cross-match service (<http://cdsxmatch.u-strasbg.fr/#tab=xmatch&>) provided by CDS, Strasbourg.

REFERENCES

- Awadalla, N. S., & Hanna, M. A. 2005, *Journal of Korean Astronomical Society*, 38, 43, doi: [10.5303/JKAS.2005.38.2.043](https://doi.org/10.5303/JKAS.2005.38.2.043)
- Bellm, E. C., Kulkarni, S. R., Barlow, T., et al. 2019, *PASP*, 131, 068003, doi: [10.1088/1538-3873/ab0c2a](https://doi.org/10.1088/1538-3873/ab0c2a)
- Binnendijk, L. 1970, *Vistas in Astronomy*, 12, 217, doi: [10.1016/0083-6656\(70\)90041-3](https://doi.org/10.1016/0083-6656(70)90041-3)
- Chen, X., de Grijs, R., & Deng, L. 2016, *ApJ*, 832, 138, doi: [10.3847/0004-637X/832/2/138](https://doi.org/10.3847/0004-637X/832/2/138)
- Chen, X., Deng, L., de Grijs, R., Wang, S., & Feng, Y. 2018a, *ApJ*, 859, 140, doi: [10.3847/1538-4357/aabe83](https://doi.org/10.3847/1538-4357/aabe83)
- Chen, X., Wang, S., Deng, L., de Grijs, R., & Yang, M. 2018b, *ApJS*, 237, 28, doi: [10.3847/1538-4365/aad32b](https://doi.org/10.3847/1538-4365/aad32b)
- Chen, X., Wang, S., Deng, L., et al. 2020, *ApJS*, 249, 18, doi: [10.3847/1538-4365/ab9cae](https://doi.org/10.3847/1538-4365/ab9cae)
- Christy, C. T., Jayasinghe, T., Stanek, K. Z., et al. 2023, *MNRAS*, 519, 5271, doi: [10.1093/mnras/stac3801](https://doi.org/10.1093/mnras/stac3801)
- Clarke, D. 2002, *A&A*, 386, 763, doi: [10.1051/0004-6361:20020258](https://doi.org/10.1051/0004-6361:20020258)
- Conroy, K. E., Prša, A., Stassun, K. G., et al. 2014, *AJ*, 147, 45, doi: [10.1088/0004-6256/147/2/45](https://doi.org/10.1088/0004-6256/147/2/45)
- Dal, H. A., & Sipahi, E. 2013, *PASA*, 30, e016, doi: [10.1017/pasa.2012.016](https://doi.org/10.1017/pasa.2012.016)
- Debski, B. 2022, *MNRAS*, 516, 5003, doi: [10.1093/mnras/stac2190](https://doi.org/10.1093/mnras/stac2190)
- Ding, X., Ji, K., Li, X., et al. 2022, *AJ*, 164, 200, doi: [10.3847/1538-3881/ac8e66](https://doi.org/10.3847/1538-3881/ac8e66)
- Ding, X., Ji, K.-F., & Li, X.-Z. 2021, *PASJ*, 73, 786, doi: [10.1093/pasj/psab042](https://doi.org/10.1093/pasj/psab042)
- Drake, A. J., Djorgovski, S. G., Mahabal, A., et al. 2009, *ApJ*, 696, 870, doi: [10.1088/0004-637X/696/1/870](https://doi.org/10.1088/0004-637X/696/1/870)
- Drake, A. J., Graham, M. J., Djorgovski, S. G., et al. 2014, *ApJS*, 213, 9, doi: [10.1088/0067-0049/213/1/9](https://doi.org/10.1088/0067-0049/213/1/9)
- Egger, O. J. 1967, *MNRAS*, 70, 111
- Eker, Z., Demircan, O., Bilir, S., & Karataş, Y. 2006, *MNRAS*, 373, 1483, doi: [10.1111/j.1365-2966.2006.11073.x](https://doi.org/10.1111/j.1365-2966.2006.11073.x)
- Esa, . 1997, *VizieR Online Data Catalog*, I/239
- Ferreira, T., Saito, R. K., Minniti, D., et al. 2019, *MNRAS*, 486, 1220, doi: [10.1093/mnras/stz878](https://doi.org/10.1093/mnras/stz878)
- Gaia Collaboration, Vallenari, A., Brown, A. G. A., et al. 2023, *A&A*, 674, A1, doi: [10.1051/0004-6361/202243940](https://doi.org/10.1051/0004-6361/202243940)
- Gazeas, K., & Stepień, K. 2008, *MNRAS*, 390, 1577, doi: [10.1111/j.1365-2966.2008.13844.x](https://doi.org/10.1111/j.1365-2966.2008.13844.x)
- Gazeas, K. D., & Niarchos, P. G. 2006, *MNRAS*, 370, L29, doi: [10.1111/j.1745-3933.2006.00182.x](https://doi.org/10.1111/j.1745-3933.2006.00182.x)
- Gazeas, K. D., Loukaidou, G. A., Niarchos, P. G., et al. 2021, *MNRAS*, 502, 2879, doi: [10.1093/mnras/stab234](https://doi.org/10.1093/mnras/stab234)
- Gettel, S. J., Geske, M. T., & McKay, T. A. 2006, *AJ*, 131, 621, doi: [10.1086/498016](https://doi.org/10.1086/498016)
- Graczyk, D., Soszyński, I., Poleski, R., et al. 2011, *AcA*, 61, 103, doi: [10.48550/arXiv.1108.0446](https://doi.org/10.48550/arXiv.1108.0446)
- Heinze, A. N., Tonry, J. L., Denneau, L., et al. 2018, *AJ*, 156, 241, doi: [10.3847/1538-3881/aae47f](https://doi.org/10.3847/1538-3881/aae47f)
- Jayasinghe, T., Kochanek, C. S., Stanek, K. Z., et al. 2018, *MNRAS*, 477, 3145, doi: [10.1093/mnras/sty838](https://doi.org/10.1093/mnras/sty838)
- Jayasinghe, T., Stanek, K. Z., Kochanek, C. S., et al. 2019a, *MNRAS*, 486, 1907, doi: [10.1093/mnras/stz844](https://doi.org/10.1093/mnras/stz844)
- . 2019b, *MNRAS*, 485, 961, doi: [10.1093/mnras/stz444](https://doi.org/10.1093/mnras/stz444)
- . 2020a, *MNRAS*, 493, 4045, doi: [10.1093/mnras/staa518](https://doi.org/10.1093/mnras/staa518)
- . 2020b, *MNRAS*, 491, 13, doi: [10.1093/mnras/stz2711](https://doi.org/10.1093/mnras/stz2711)
- Jayasinghe, T., Kochanek, C. S., Stanek, K. Z., et al. 2021, *MNRAS*, 503, 200, doi: [10.1093/mnras/stab114](https://doi.org/10.1093/mnras/stab114)
- Jiang, D. 2020, *MNRAS*, 492, 2731, doi: [10.1093/mnras/stz3578](https://doi.org/10.1093/mnras/stz3578)
- Kirk, B., Conroy, K., Prša, A., et al. 2016, *AJ*, 151, 68, doi: [10.3847/0004-6256/151/3/68](https://doi.org/10.3847/0004-6256/151/3/68)
- Kopal, Z. 1959, *Close binary systems*

- Kuiper, G. P. 1941, *ApJ*, 93, 133, doi: [10.1086/144252](https://doi.org/10.1086/144252)
- Lafler, J., & Kinman, T. D. 1965, *ApJS*, 11, 216, doi: [10.1086/190116](https://doi.org/10.1086/190116)
- Latković, O., Čeki, A., & Lazarević, S. 2021, *ApJS*, 254, 10, doi: [10.3847/1538-4365/abeb23](https://doi.org/10.3847/1538-4365/abeb23)
- Li, K., Gao, X., Liu, X.-Y., et al. 2022, *AJ*, 164, 202, doi: [10.3847/1538-3881/ac8ff2](https://doi.org/10.3847/1538-3881/ac8ff2)
- Li, K., Xia, Q.-Q., Kim, C.-H., et al. 2021, *ApJ*, 922, 122, doi: [10.3847/1538-4357/ac242f](https://doi.org/10.3847/1538-4357/ac242f)
- Li, L., Zhang, F., Han, Z., & Jiang, D. 2007, *ApJ*, 662, 596, doi: [10.1086/517909](https://doi.org/10.1086/517909)
- Li, L., Zhang, F., Han, Z., Jiang, D., & Jiang, T. 2008, *MNRAS*, 387, 97, doi: [10.1111/j.1365-2966.2008.12736.x](https://doi.org/10.1111/j.1365-2966.2008.12736.x)
- Li, X.-Z., & Liu, L. 2021, *NewA*, 84, 101539, doi: [10.1016/j.newast.2020.101539](https://doi.org/10.1016/j.newast.2020.101539)
- Li, X.-Z., Liu, L., & Zhu, L.-Y. 2020, *PASJ*, 72, 103, doi: [10.1093/pasj/psaa104](https://doi.org/10.1093/pasj/psaa104)
- Liu, L., Qian, S. B., & Xiong, X. 2018, *MNRAS*, 474, 5199, doi: [10.1093/mnras/stx3138](https://doi.org/10.1093/mnras/stx3138)
- Loukaidou, G. A., Gazeas, K. D., Palafouta, S., et al. 2022, *MNRAS*, 514, 5528, doi: [10.1093/mnras/stab3424](https://doi.org/10.1093/mnras/stab3424)
- Lucy, L. B. 1968a, *ApJ*, 151, 1123, doi: [10.1086/149510](https://doi.org/10.1086/149510)
- . 1968b, *ApJ*, 153, 877, doi: [10.1086/149712](https://doi.org/10.1086/149712)
- Maceroni, C., & van't Veer, F. 1996, *A&A*, 311, 523
- Mateo, N. M., & Rucinski, S. M. 2017, *AJ*, 154, 125, doi: [10.3847/1538-3881/aa8453](https://doi.org/10.3847/1538-3881/aa8453)
- Molík, P. 1998, in *20th Stellar Conference of the Czech and Slovak Astronomical Institutes*, ed. J. Dusek, 81
- Mowlavi, N., Lecoer-Taïbi, I., Holl, B., et al. 2017, *A&A*, 606, A92, doi: [10.1051/0004-6361/201730613](https://doi.org/10.1051/0004-6361/201730613)
- Mowlavi, N., Holl, B., Lecoer-Taïbi, I., et al. 2023, *A&A*, 674, A16, doi: [10.1051/0004-6361/202245330](https://doi.org/10.1051/0004-6361/202245330)
- Paczyński, B., Szczygiel, D. M., Pilecki, B., & Pojmański, G. 2006, *MNRAS*, 368, 1311, doi: [10.1111/j.1365-2966.2006.10223.x](https://doi.org/10.1111/j.1365-2966.2006.10223.x)
- Pawlak, M., Soszyński, I., Udalski, A., et al. 2016, *AcA*, 66, 421, doi: [10.48550/arXiv.1612.06394](https://doi.org/10.48550/arXiv.1612.06394)
- Pojmanski, G. 1997, *AcA*, 47, 467, <https://arxiv.org/abs/astro-ph/9712146>
- Prša, A., Guinan, E. F., Deviney, E. J., et al. 2008, *ApJ*, 687, 542, doi: [10.1086/591783](https://doi.org/10.1086/591783)
- Prša, A., Batalha, N., Slawson, R. W., et al. 2011, *AJ*, 141, 83, doi: [10.1088/0004-6256/141/3/83](https://doi.org/10.1088/0004-6256/141/3/83)
- Prša, A., Conroy, K. E., Horvat, M., et al. 2016, *ApJS*, 227, 29, doi: [10.3847/1538-4365/227/2/29](https://doi.org/10.3847/1538-4365/227/2/29)
- Prša, A., Kochoska, A., Conroy, K. E., et al. 2022, *ApJS*, 258, 16, doi: [10.3847/1538-4365/ac324a](https://doi.org/10.3847/1538-4365/ac324a)
- Qian, S.-B., He, J.-J., Zhang, J., et al. 2017, *Research in Astronomy and Astrophysics*, 17, 087, doi: [10.1088/1674-4527/17/8/87](https://doi.org/10.1088/1674-4527/17/8/87)
- Qian, S. B., Zhang, J., He, J. J., et al. 2018, *ApJS*, 235, 5, doi: [10.3847/1538-4365/aaa601](https://doi.org/10.3847/1538-4365/aaa601)
- Qian, S.-B., Zhu, L.-Y., Liu, L., et al. 2020, *Research in Astronomy and Astrophysics*, 20, 163, doi: [10.1088/1674-4527/20/10/163](https://doi.org/10.1088/1674-4527/20/10/163)
- Ren, F., de Grijs, R., Zhang, H., et al. 2021, *AJ*, 161, 176, doi: [10.3847/1538-3881/abe30e](https://doi.org/10.3847/1538-3881/abe30e)
- Rucinski, S. M. 1994, *PASP*, 106, 462, doi: [10.1086/133401](https://doi.org/10.1086/133401)
- Shappee, B. J., Prieto, J. L., Grupe, D., et al. 2014, *ApJ*, 788, 48, doi: [10.1088/0004-637X/788/1/48](https://doi.org/10.1088/0004-637X/788/1/48)
- Skarka, M., Žák, J., Fedurco, M., et al. 2022, *A&A*, 666, A142, doi: [10.1051/0004-6361/202244037](https://doi.org/10.1051/0004-6361/202244037)
- Soszyński, I., Pawlak, M., Pietrukowicz, P., et al. 2016, *AcA*, 66, 405. <https://arxiv.org/abs/1701.03105>
- Stepień, K. 2009, *MNRAS*, 397, 857, doi: [10.1111/j.1365-2966.2009.14981.x](https://doi.org/10.1111/j.1365-2966.2009.14981.x)
- Stepien, K. 2006, *AcA*, 56, 199, <https://arxiv.org/abs/astro-ph/0510464>
- Stepień, K. 2011, *AcA*, 61, 139, <https://arxiv.org/abs/1105.2645>
- Sun, W., Chen, X., Deng, L., & de Grijs, R. 2020, *ApJS*, 247, 50, doi: [10.3847/1538-4365/ab7894](https://doi.org/10.3847/1538-4365/ab7894)
- Tylenda, R., Hajduk, M., Kamiński, T., et al. 2011, *A&A*, 528, A114, doi: [10.1051/0004-6361/201016221](https://doi.org/10.1051/0004-6361/201016221)
- Udalski, A., Kubiak, M., Szymanski, M., et al. 1994, *AcA*, 44, 317
- Udalski, A., Szymanski, M., Kaluzny, J., Kubiak, M., & Mateo, M. 1992, *AcA*, 42, 253
- Van Hamme, W., & Wilson, R. E. 2007, *ApJ*, 661, 1129, doi: [10.1086/517870](https://doi.org/10.1086/517870)
- Webbink, R. F. 2003, in *Astronomical Society of the Pacific Conference Series*, Vol. 293, *3D Stellar Evolution*, ed. S. Turcotte, S. C. Keller, & R. M. Cavallo, 76, <https://arxiv.org/abs/astro-ph/0304420>
- Wilson, R. E. 1990, *ApJ*, 356, 613, doi: [10.1086/168867](https://doi.org/10.1086/168867)
- . 2012, *AJ*, 144, 73, doi: [10.1088/0004-6256/144/3/73](https://doi.org/10.1088/0004-6256/144/3/73)
- Wilson, R. E., & Deviney, E. J. 1971, *ApJ*, 166, 605, doi: [10.1086/150986](https://doi.org/10.1086/150986)
- Wilson, R. E., Van Hamme, W., & Terrell, D. 2010, *ApJ*, 723, 1469, doi: [10.1088/0004-637X/723/2/1469](https://doi.org/10.1088/0004-637X/723/2/1469)
- Woźniak, P. R., Vestrand, W. T., Akerlof, C. W., et al. 2004, *AJ*, 127, 2436, doi: [10.1086/382719](https://doi.org/10.1086/382719)
- Wright, E. L., Eisenhardt, P. R. M., Mainzer, A. K., et al. 2010, *AJ*, 140, 1868, doi: [10.1088/0004-6256/140/6/1868](https://doi.org/10.1088/0004-6256/140/6/1868)
- Yakut, K., & Eggleton, P. P. 2005, *ApJ*, 629, 1055, doi: [10.1086/431300](https://doi.org/10.1086/431300)
- Yang, Y.-G., & Qian, S.-B. 2015, *AJ*, 150, 69, doi: [10.1088/0004-6256/150/3/69](https://doi.org/10.1088/0004-6256/150/3/69)
- Yıldız, M. 2014, *MNRAS*, 437, 185, doi: [10.1093/mnras/stt1874](https://doi.org/10.1093/mnras/stt1874)

Yildiz, M., & Doğan, T. 2013, MNRAS, 430, 2029,

doi: [10.1093/mnras/stt028](https://doi.org/10.1093/mnras/stt028)

Zhang, J., Qian, S.-B., Wu, Y., & Zhou, X. 2019, ApJS,

244, 43, doi: [10.3847/1538-4365/ab442b](https://doi.org/10.3847/1538-4365/ab442b)

Zhang, X.-D., Qian, S.-B., & Liao, W.-P. 2020, MNRAS,
492, 4112, doi: [10.1093/mnras/staa079](https://doi.org/10.1093/mnras/staa079)

Zhou, X., Qian, S. B., Zhang, J., et al. 2016, ApJ, 817, 133,
doi: [10.3847/0004-637X/817/2/133](https://doi.org/10.3847/0004-637X/817/2/133)

Zhu, L.-Y., Zhao, E.-G., & Zhou, X. 2016, Research in
Astronomy and Astrophysics, 16, 68,
doi: [10.1088/1674-4527/16/4/068](https://doi.org/10.1088/1674-4527/16/4/068)